Engineering Geology 313 (2023) 106962

Contents lists available at ScienceDirect

Engineering Geology

journal homepage: www.elsevier.com/locate/enggeo

Assessing water-induced changes in tensile behaviour of porous limestones by means of uniaxial direct pull test and indirect methods

Álvaro Rabat *, Roberto Tomás, Miguel Cano

Departamento de Ingeniería Civil, Escuela Politécnica Superior, Universidad de Alicante, P.O. Box 99, E-03080 Alicante, Spain

ARTICLE INFO

Keywords:
Uniaxial tensile properties
Water-induced weakening
Porous limestone
Brazilian test
Point load test
Uniaxial direct pull test

ABSTRACT

Understanding the uniaxial tensile behaviour of rocks and its water-induced variation are key issues for designing effective mining and civil engineering structures and for assessing numerous geotechnical hazards. However, these aspects remain poorly analysed because conducting uniaxial direct pull tests is a difficult and time-consuming laboratory task that requires the use of sophisticated equipment and complex rock sample preparation and processing. This work attempts to expand knowledge by determining several tensile properties of three porous limestone lithotypes under dry and water-saturated conditions through two different approaches: by conducting direct tensile tests and by means of indirect methods (i.e. Brazilian and point load tests). The results revealed that water saturation generated important reductions in their uniaxial tensile strength (UTS), tensile elastic modulus (E_t), Brazilian tensile strength (BTS) and point load strength index ($I_{s(50)}$). In addition, their petrological characteristics and mineralogical composition are used to discuss the main causes of the observed tensile softening. Furthermore, highly accurate correlation functions were established between the direct tensile strength parameters (UTS and E_t) and the indirect ones (BTS and $I_{s(50)}$) for the whole set of tested rocks. The proposed relationships are a novel and useful contribution to geomechanics because they enable the estimation of pure tensile parameters using alternative, cheap, rapid and versatile tests.

1. Introduction

Numerous researchers have investigated the compressive behaviour of rocks under different moisture conditions. They have demonstrated that uniaxial compressive strength (UCS), compressive Young's modulus (E_c) and shear strength parameters of sedimentary rocks can be significantly reduced after their full and partial water saturation (e.g. Hawkins and McConnell, 1992; Vásárhelyi, 2005; Erguler and Ulusay, 2009; Shakoor and Barefield, 2009; Kim and Changani, 2016; Rabat et al., 2020a, 2020b, 2020c, 2021). However, the mechanical response of these geomaterials under tensile stress and its water-induced variation have been poorly analysed due to the difficulties in tensile testing (Briševac et al., 2015; Hashiba and Fukui, 2015; Okubo and Fukui, 1996). This is a relevant research topic because the tensile failure of rock masses is the main failure mode in engineering practice (Huang et al., 2021; Liao et al., 1997; Zhang et al., 2018). In particular, an understanding of the rock behaviour under tension is of paramount importance in the design, execution and stability analysis of underground structures such as galleries, mining roofs, storage caverns, tunnel boring, drilling or blasting (Coviello et al., 2005).

By definition, tensile strength is the failure stress of a rock sample in pure uniaxial tensile loading (Tufekci et al., 2016). Hence, the direct pull test, in which a cylindrical rock specimen is loaded to failure by a tensile axial force, is the ideal method for its measurement (Dai et al., 2010) (Fig. 1a). However, in laboratory practice, determining the UTS in a correct and accurate way is challenging due to several drawbacks. For example, bending effects caused by instrumental misalignments are difficult to avoid (Dai et al., 2010). Also, stress concentration around the grips can produce an early and undesirable failure around the end of the specimens. Furthermore, even when the failure happens in the central zone of the sample, the stress state might be non-uniform throughout the cross section (Coviello et al., 2005). To overcome the above-mentioned difficulties, researchers could follow different strategies to obtain the tensile strength of rocks, for example to implement technical improvements in the execution of direct tensile tests or to use indirect methods.

Various technological innovations have been devised to reduce the problems related to the practical implementation of direct tensile strength tests. Fairhurst (1961) recommended testing cylindrical specimens glued directly to end caps of the same diameter by means of epoxy cements in order to decrease the stress concentrations at the ends of the sample. With the same purpose, Brace (1964) and Hoek (1964) proposed

* Corresponding author.
E-mail address: alvaro.rabat@ua.es (Á. Rabat).

https://doi.org/10.1016/j.enggeo.2022.106962
Received 1 June 2022; Received in revised form 23 November 2022; Accepted 1 December 2022
Available online 5 December 2022

List of symbols

BT	Brazilian test
BTS	Brazilian tensile strength
CN	Crossed nicols
c_p	Peak cohesion
d_M	Mean pore diameter
E_c	Compressive Young's modulus
E_t	Tensile elastic modulus
$I_{s(50)}$	Point load strength index
K_{BTS}	Ratio between the BTS values obtained under water-saturated and dry conditions
K_{Et}	Ratio between the E_t values obtained under water-saturated and dry conditions
$K_{Is(50)}$	Ratio between the $I_{s(50)}$ values obtained under water-saturated and dry conditions
K_{UTS}	Ratio between the UTS values obtained under water-saturated and dry conditions
LVDT	Linear variable differential transducer
m_i	Hoek-Brown constant
MAE	Mean absolute error
MAPE	Mean absolute percentage error
MSE	Mean square error
M_z	Mean grain size
p	Total porosity
p_o	Open porosity
PLT	Point load test
PN	Parallel nicols
UCS	Uniaxial compressive strength
UTS	Uniaxial tensile strength
R^2	Coefficient of determination
R_{BI}	Ratio between BTS and $I_{s(50)}$
R_{EB}	Ratio between E_t and BTS
R_{EU}	Ratio between E_t and UTS
R_{UB}	Ratio between UTS and BTS
R_{UI}	Ratio between UTS and $I_{s(50)}$
ρ_b	Bulk density
σ_{ci}	Hoek-Brown strength parameter
φ_p	Internal friction angle

the use of curved dog-bone shaped specimens and split grips. Also, machining a notch on the rock surface has been another technique used for forcing the fracture in the central zone of the sample (Coviello et al., 2005). The utilisation of universal or ball joints to allow the sample to centre itself during loading as well as performing biaxial extension tests are solutions to avoid that the sample can fail in torsion and that the load transfer instrument twists during loading (Perras and Diederichs, 2014). Furthermore, with the aim of using conventional load frames, Gorski (1993) and Klanphumeesri (2010) designed compression load converters, which are devices capable of transforming the downward compressive load into an upward tension pull on dog-bone specimens. However, these developments make direct tensile testing expensive and time-consuming (Efe et al., 2021).

Alternatively, many indirect methods have been proposed for obtaining the tensile strength of rocks, such as the ring test (Hobbs, 1965), the three- and four-points beam bending tests (ASTM, 2018a, 2018b), the sleeve-fracturing test (Brenne et al., 2013), the modified tension test (Franklin and Dusseault, 1989), the Luong test (Luong, 1990), the wedge splitting test (Garcia-Fernandez et al., 2016; Guan et al., 2018), the Brazilian test (BT) (ASTM, 2008) or the point load test (PLT) (Franklin, 1985). Among them, the last two mentioned methods are the most widely used due to the ease of specimen preparation, simplicity and low cost (Rabat et al., 2020; Unlu and Yilmaz, 2014) (Fig. 1b and c). However, the tensile strength values obtained using BT and PLT techniques are not strictly comparable with those provided by the direct tensile test, due to the tensile stress normal to the breakage plane is accompanied by a compressive component in the loading direction (Broch and Franklin, 1972). Furthermore, numerical and experimental research has indicated that the crack initiation point may be located away from the centre of the test sample (Al-Derbi and De Freitas, 1999; Li and Wong, 2013).

A compilation of the values of the ratio between UTS and BTS (R_{UB}) obtained in previous studies for different geomaterials can be seen in Table 1. Its examination shows that BTS test commonly overestimates the true tensile strength of intact rocks, although the opposite has also been reported in a limited number of cases. Furthermore, the R_{UB} varies largely depending on lithology. In this line, for practical applications, Perras and Diederichs (2014) proposed to adopt R_{UB} values of 0.7 for sedimentary, 0.8 for igneous and 0.9 for metamorphic rocks.

The value of the ratio between UTS and $I_{s(50)}$ (R_{UI}) has been scarcely inspected. Particularly, Zhang (2017) suggested that a general value of R_{UI} equal to 1.5 could be used for preliminary works. In the same vein, the deficit of experimental data on rock deformability under tensile stresses (Hashiba and Fukui, 2015; Okubo and Fukui, 1996) has prevented that preceding works analysed the values of the ratio between E_t and other tensile strength parameters, such as UTS (R_{EU}), BTS (R_{EB}) or $I_{s(50)}$ (R_{EI}). By contrast, more abundant research has been conducted to determine the values of the ratio between BTS and $I_{s(50)}$ (R_{BI}), using

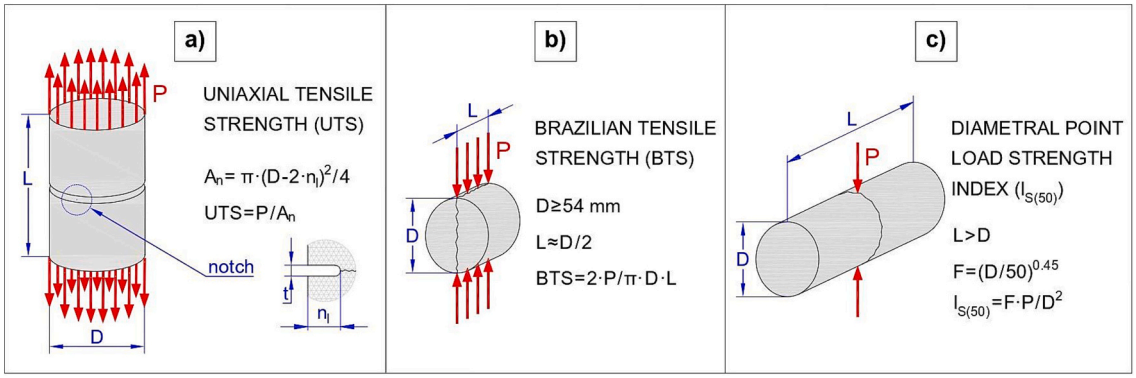

Fig. 1. Determining the direct and indirect tensile strength parameters: (a) uniaxial tensile strength (UTS), (b) Brazilian tensile strength (BTS) and (c) diametral point load strength index ($I_{s(50)}$).

Table 1
Compilation of the values of the uniaxial tensile strength (UTS), Brazilian tensile strength (BTS) and the ratio between both properties (R_{UB}) obtained in different rock types by previous studies.

Authors	Rock type	UTS (MPa)	BTS (MPa)	R_{UB} (UTS/BTS)
Berenbaum and Brodie (1959)	Paris Plaster	3.79	3.03	1.25
Jaeger (1967)	Bowral Trachyte	13.72	12.00	1.14
	Gosford Sandstone	3.59	3.72	0.97
	Carrara Marble	6.89	8.72	0.79
Mellor and Hawkes (1971)	Indiana Limestone	5.86	6.21	0.94
	Barre Granite	13.45	14.34	0.94
Ramana and Sarma (1987)	Kolar Schist	14.29	13.87	1.03
	Dolomite	6.93	8.49	0.82
	Vein Quartz	13.88	16.28	0.85
	Jawaar Schist	10.93	10.33	1.06
	Dolomite (layered texture)	4.51	6.18	0.73
	Hyderabad Granite	7.63	7.26	1.05
Andreev (1991)	White Gypsum	1.42	1.29	1.10
	Grey Gypsum	1.75	1.99	0.88
	Vitosha Syenite	20.5	21.05	0.97
Martin (1993)	Lac du Bonnet Granite	6.90	8.80	0.78
Okubo and Fukui (1996)	Sanjome Andesite	6.20	6.30	0.98
	Tage Tuff	9.60	11.00	0.87
Alehossein and Boland (2004)	Granite	11.11	13.46	0.83
Coviello et al. (2005)	Gravina Calcarenite	0.69	0.64	1.08
Gorski et al. (2007)	Medium-grained Granodiorite	11.06	18.96	0.58
Efimov (2009)	Ufalei Marble	5.90	6.90	0.86
Fuenkajorn and Klanphumeesri (2010)	Phu Phan Sandstone	6.49	10.68	0.61
	Saraburi Marble	6.33	8.02	0.79
	Saraburi Limestone	9.31	10.90	0.85
Fahimifar and Malekpour (2012)	Isotropic Limestone	3.20	4.41	0.73
Unlu and Yilmaz (2014)	Andesite	3.90	7.10	0.55
	Sandstone	6.80	8.90	0.76
	Limestone	11.90	11.80	1.01
	Basalt	10.00	13.00	0.77
Tufekci et al. (2016)	Denizli Travertine	3.02	3.64	0.83
Zhang et al. (2018)	Mengdigou Ganite	5.68	8.01	0.71
	Xiluodu Basalt	7.34	11.16	0.66
	Xiluodu Breccia Lava	5.81	9.62	0.60
	Dagangshan Granite	5.04	7.64	0.66
	Dagangshan Diabase	7.39	11.58	0.64
	Jinping-I Marble	2.77	4.15	0.67
Cacciari and Futai (2018)	Marble	1.70	2.70	0.63
	White Granite	4.92	6.51	0.76
	Red Granite	6.66	7.76	0.86
	Andesite	13.91	16.77	0.83
Demirdag et al. (2019)	Granite	5.27	9.54	0.55
Gong et al. (2019)	Red Sandstone	4.19	6.67	0.63
Huang et al. (2021)	Granite	7.70	8.74	0.88
	Marble	5.84	6.84	0.85
	Diabase	5.67	6.61	0.86
Rao et al. (2021)	Fine-grain Red Sandstone	2.43	4.85	0.50
Efe et al. (2021)	Lymra Limestone	3.45	5.34	0.65
	Fine Crystalline Marble	3.19	7.69	0.41
	Coarse Crystalline Marble	2.85	5.24	0.54
	Tuff	1.36	2.05	0.66
	Andesite	4.88	9.41	0.52
	Granite	5.27	9.54	0.55
	Diabase	8.87	15.87	0.56

linear, exponential and power functions to correlate both indirect tensile indexes for different rock types, as reflected in Table 2.

The study of the water-induced variations in tensile properties of rocks has been addressed by relatively few investigations. They have revealed that rocks (especially the sedimentary types) can undergo important reductions of UTS, tensile elastic modulus (E_t), BTS and $I_{s(50)}$ due to water saturation (Broch, 1983; Dube and Singh, 1972; Erguler and Ulusay, 2009; Gholami and Rasouli, 2014; Hashiba and Fukui, 2015; Hawkes et al., 1973; Kahraman, 2014; Karakul and Ulusay, 2013; Kohno and Maeda, 2012; Ojo and Brook, 1990; Parate, 1973; Sadeghiamirshahidi and Vitton, 2019). A summary of the softening coefficients (K), that represent the ratios between the values of each tensile property in water-saturated and dry conditions obtained in different geomaterials by earlier academics, are shown in Table 3.

In this research, the tensile behaviour of porous calcareous rocks is obtained by performing direct and indirect tests. In particular, properties such as UTS, E_t, BTS and $I_{s(50)}$ are determined in dry and fully water-saturated samples of three limestone lithotypes. Furthermore, relationships between the above-mentioned parameters are established to find out the suitability of the BT and diametral PLT methods for indirectly determining the true tensile strength and stiffness values of these rocks. In addition, the different tensile softening coefficients of these geomaterials are presented and the possible mechanisms controlling the water-induced weakening are discussed based on their physical properties and microstructure.

2. Materials and testing program

2.1. Used rocks and specimen preparation

Tested rocks are three lithotypes of a porous sandy limestone of the Middle-Upper Miocene from south-eastern Spain (Alicante). They were collected from a working quarry placed around the village of Elda and owned by a local company that marketed them as building materials under the name of *Blue* (L-1), *Beige* (L-2) and *Diamond* (L-3) *Bateig* stones.

From a petrological point of view, they are calcarenites mostly constituted of fossils (55–60%), such as foraminifera, molluscs, bryozoans and echinoderms. Their main terrigenous components (10–20%) are monocrystalline and polycrystalline quartz, dolomite, potassium feldspar and phyllosilicates. Their principal ortochemical constituents (15–20%) are a micritic matrix and sparitic cement (Fig. 2) (Fort et al., 2010; Ordoñez et al., 1994; Ordóñez et al., 1997).

The petrological characteristics and physico-mecanical properties of these geomaterials under compressive conditions have been extensively analysed by Rabat et al. (2020c) (Fig. 2). In broad outline, these rocks exhibit a mean pore diameter of 0.2–3.0 μm, and a mean grain size of

Table 2
Relationships between Brazilian tensile strength (BTS) and point load strength index ($I_{s(50)}$) found in different rock types by preceding researchers.

Authors	Rock type	Correlation function	R^2
Grasso et al. (1992)	Calcareous mudstone	$BTS = 1.01 \bullet e^{0.47 \bullet I_{s(50)}}$	0.93
Sulukcu and Ulusay (2001)	Different Turkish rocks	$BTS = 2.30 \bullet I_{s(50)}$	0.64
Heidari et al. (2012)	Dry gypsiferous rock	$BTS = 1.77 \bullet I_{s(50)} + 2.57$	0.87
	Saturated gypsiferous rock	$BTS = 2.90 \bullet I_{s(50)} + 1.10$	0.77
Raj and Pedram (2015)	Basalt and rhyolite	$BTS = 11 \bullet I_{s(50)}$	0.81
Fereidooni (2016)	Hornfels	$BTS = 2.28 \bullet I_{s(50)} - 4.66$	0.95
Minaeian and Ahangari (2017)	Weak conglomerate	$BTS = I_{s(50)}^{0.826}$	0.78
Sari (2018)	Different lithologies	$BTS = 2.04 \bullet I_{s(50)}^{0.835}$	0.85
Sadeghiamirshahidi and Vitton (2019)	Dry gypsum	$BTS = 2.92 \bullet I_{s(50)}$	0.35
	Saturated gypsum	$BTS = 2.39 \bullet I_{s(50)}$	0.93

Table 3
Summary of the softening coefficients of tensile properties (K_{UTS}, K_{Et}, K_{BTS} and $K_{Is(50)}$) obtained in different rock types by earlier academics.

Authors	Rock type	Softening coefficients (K)	
Hawkes et al. (1973)	Berea Sandstone	$K_{UTS} = \frac{UTS_{sat}}{UTS_{dry}}$	0.76–0.84
	Indiana Limestone		0.71
	Barre Granite		0.80
Parate (1973)	Fine-grained Limestone		0.40
Ojo and Brook (1990)	Woodkirk Sandstone		0.49
Hashiba and Fukui (2015)	Sanjome Andesite		0.42
	Inada Granite		0.92
	Kawazu Tuff		0.47
	Komatsu Andesite		0.66
Hawkes et al. (1973)	Berea Sandstone	$K_{E_t} = \frac{E_{t\,sat}}{E_{t\,dry}}$	0.85
	Indiana Limestone		0.51
	Barre Granite		0.73
Hashiba and Fukui (2015)	Sanjome Andesite		0.54
Dube and Singh (1972)	Sandstone	$K_{BTS} = \frac{BTS_{sat}}{BTS_{dry}}$	0.51–0.82
Erguler and Ulusay (2009)	Siltstone		0.28
	Marl		0.25
	Mudstone		0.34
	Tuff		0.06
Karakul and Ulusay (2013)	Marl		0.34
	Sandstone		0.43
	Andesite		0.53
	Limestone		0.48
	Ignimbrite		0.23
Gholami and Rasouli (2014)	Iranian slate		0.79
Sadeghiamirshahidi and Vitton (2019)	Gypsum		0.65
Broch (1983)	Sandstone	$K_{I_{s(50)}} = \frac{I_{s(50)_{sat}}}{I_{s(50)_{dry}}}$	0.82–0.92
	Limestone		0.93
	Siltstone		0.88
	Granite		0.78–0.85
	Gneiss		0.53–0.82
	Gabbro		0.62–0.84
	Quartz-Diorite		0.78–0.94
	Schist		0.77
	Diorite		0.70
Kohno and Maeda (2012)	Dacite		0.73–0.85
	Fine Tuff		0.04–0.61
	Welded Tuff		0.34–0.46
	Pumice Tuff		0.18–0.57
	Lapilli Tuff		0.27–0.61
Kahraman (2014)	Pyroclastic rocks		0.65
Sadeghiamirshahidi and Vitton (2019)	Gypsum		0.46

0.2–0.4 mm, a bulk density of 2.1–2.4 g/cm^3, an open porosity of 10.7–17.9%, and a total porosity of 14.9–23.8%. Furthermore, they display a wide range of values of their compressive mechanical parameters depending on their water content: an UCS of 14.7–83.0 MPa, an E_c of 6.4–12.7 GPa, a peak cohesion (c_p) of 5.9–21.6 MPa, an internal friction angle (φ_p) of 21.4–37.4°, a Hoek-Brown strength parameter (σ_{ci}) of 14.8–85.8 MPa and a Hoek-Brown constant (m_i) of 3.5–10.4. However, to date, there is a lack of scientific studies investigating their mechanical behaviour under direct tensile conditions and its relationships with indirect tensile strength parameters, which has motivated the present research.

With the aim of obtaining samples for the direct and indirect tensile strength tests, cylindrical cores were bored perpendicularly to the sedimentary bedding from unweathered and homogeneous rock blocks by using a drill rig. Then, the rock cores were cut by means of a circular saw to get specimens with the length specified in the ISRM Suggested Methods (ISRM, 2007) (Fig. 3a). For UTS tests, 12 specimens of 54 mm in diameter and 110 mm in length (4 units of each limestone lithotype) were used. The cross-section of these specimens was reduced in the middle of their length by making a circumferential notch of 4 mm in width and 12 mm in depth (Fig. 3b). This type of notch does not significantly modify the values of the tensile strength and has the advantage of ensuring the consistency in the failure pattern of the specimens, in contrast to the tests carried out with unnotched specimens (Li et al., 2017; Wang et al., 2019; Zhu et al., 2022). In addition, the bases of the specimens were surface treated to improve their adhesion with the epoxy cement that joins them to the end caps of the testing machine. For diametral PLT, 30 specimens of 28 mm in diameter and 75 mm in length (10 units of each limestone lithotype) were utilised (Fig. 3d). For BT, 36 disks of 54 mm in diameter and 27 mm in length (12 units of each limestone lithotype) were used (Fig. 3c).

Once the rock samples were prepared, they were divided into two groups. The first group was dried in an oven at 105 °C until the specimens reached a constant mass (dry samples). The second group was soaked in distilled water under vacuum conditions until the specimens reached constant water contents (4.71 ± 0.12% in L-1, 6.68 ± 0.36% in L-2 and 8.62 ± 0.40% in L-3) (fully water-saturated samples). The constant mass of the specimens was achieved in both groups after drying or soaking them during time periods <48 h. After that, the corresponding tensile strength tests were performed.

2.2. Direct tensile strength test

Testing procedures used to determine the uniaxial tensile strength parameters (UTS and E_t) of rocks can be summarised as follows (Fig. 4a): (1) Cylindrical metal caps with a thickness >15 mm were cemented to the surface treated specimen ends using a fast curing, steel-filled epoxy cement (DEVCON SF-5 M). (2) After the epoxy cement hardened sufficiently to exceed the tensile strength of the rock (time period of less than one hour), the sample was placed in a servo-controlled testing machine equipped with an axial load transducer with a capacity of 200 kN. In order to transmit a purely direct tensile stress to the specimens (absence of bending or torsional stresses), the metal caps were connected to the loading device by means of an appropriate linkage system (universal joints). (3) A tensile load on the specimen was applied continuously at a constant strain rate of $2{\cdot}10^{-6}$ s^{-1} so that the failure occurred within 5 min of loading, as required by the ISRM Suggested Method (ISRM, 1978). During the entire course of the loading process, linear variable differential transducers (LVDT) with a range of ±2.0 mm were used to measure the axial displacements both locally (in the notch zone) and globally (in the total length of the specimen). (4) The UTS was calculated as the ratio between the failure axial force and the failure cross-sectional area of the specimen. The secant E_t was obtained as the ratio between the axial tensile stress and the axial strain values at a stress level equal to 50% of the UTS.

2.3. Indirect tensile strength tests: Brazilian and point load methods

BTS tests were performed in accordance with ASTM standard (ASTM, 2008). Firstly, the rock disks were placed in direct contact with the machine bearing plates. Later, a continuously increasing compressive linear force was applied at a constant loading rate of 50 N/s such that the failure occurred within 1 to 5 min of loading. Finally, it was checked that the typical failure pattern consisting in a crack running nearly parallel to the loading direction and passing approximately through the centre of the disks was developed in all specimens (Fig. 4b).

Point load tests were carried out following the ISRM Suggested Method (Franklin, 1985). In particular, diametral tests were conducted on core specimens by gradually increasing the punctual load in such a way that failure happened within 10 to 60 s of loading. It was verified that valid failure modes happened in all samples (Fig. 4c).

3. Results and analysis

3.1. Uniaxial tensile strength (UTS) and tensile elastic modulus (E_t)

Representative examples of the stress-strain curves obtained in the three limestone lithotypes under uniaxial tensile stress are shown in

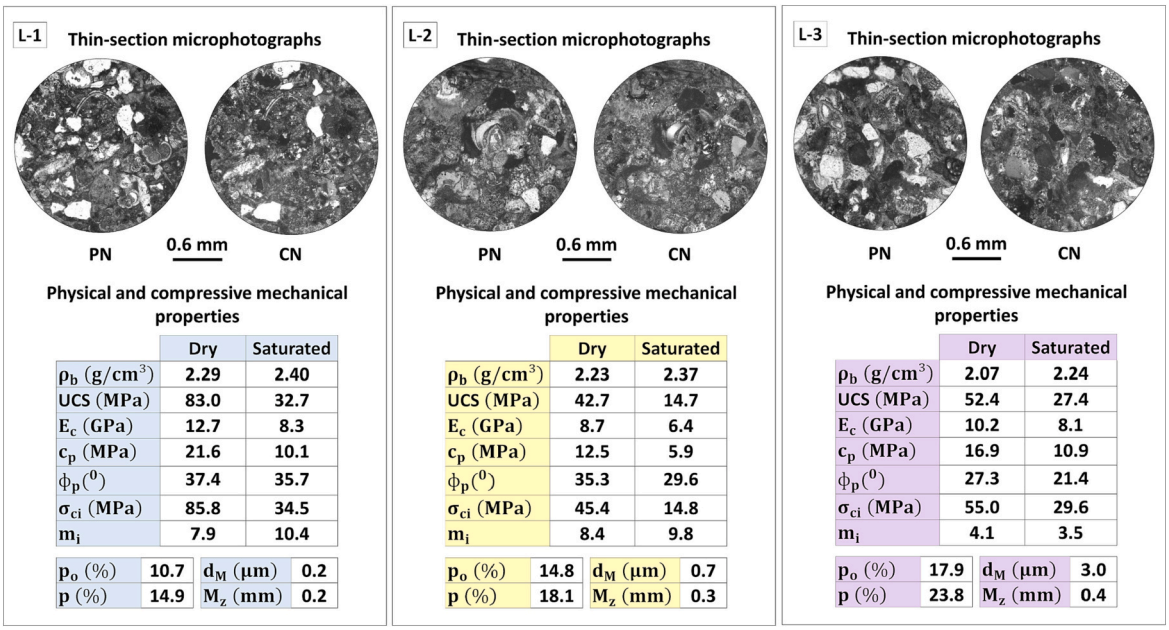

	Dry	Saturated
ρ_b (g/cm^3)	2.29	2.40
UCS (MPa)	83.0	32.7
E_c (GPa)	12.7	8.3
c_p (MPa)	21.6	10.1
ϕ_p (^{0})	37.4	35.7
σ_{ci} (MPa)	85.8	34.5
m_i	7.9	10.4

p_o (%)	10.7	d_M (μm)	0.2
p (%)	14.9	M_z (mm)	0.2

	Dry	Saturated
ρ_b (g/cm^3)	2.23	2.37
UCS (MPa)	42.7	14.7
E_c (GPa)	8.7	6.4
c_p (MPa)	12.5	5.9
ϕ_p (^{0})	35.3	29.6
σ_{ci} (MPa)	45.4	14.8
m_i	8.4	9.8

p_o (%)	14.8	d_M (μm)	0.7
p (%)	18.1	M_z (mm)	0.3

	Dry	Saturated
ρ_b (g/cm^3)	2.07	2.24
UCS (MPa)	52.4	27.4
E_c (GPa)	10.2	8.1
c_p (MPa)	16.9	10.9
ϕ_p (^{0})	27.3	21.4
σ_{ci} (MPa)	55.0	29.6
m_i	4.1	3.5

p_o (%)	17.9	d_M (μm)	3.0
p (%)	23.8	M_z (mm)	0.4

Fig. 2. Petrological characteristics and physico-mechanical properties under compressive conditions of the three limestone lithotypes (Rabat et al., 2020c). PN: Parallel nicols. CN: Crossed nicols.

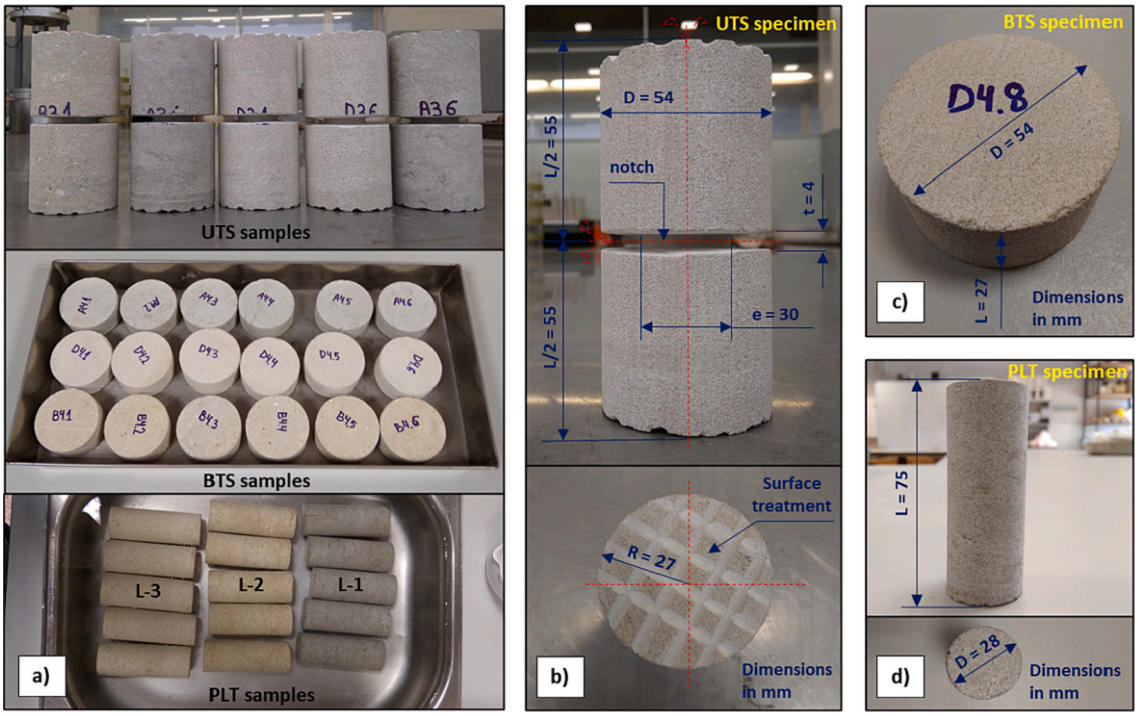

Fig. 3. Overview of some of the limestone specimens (a). Close view and dimensions of the specimens utilised for obtaining UTS, E_t (b), BTS (c) and $I_{s(50)}$ (d).

Fig. 5. The result for limestone L-1 tested in dry condition shows a linear stress-strain curve from the beginning of loading that almost remains constant until the peak stress is reached. However, in the samples tested under saturated condition, the curve of lithotype L-1 exhibits an initially linear region, which progressively decreases its slope and becomes concave downward. Lithotypes L-2 and L-3 present stress-strain curves with a quite similar shape. In dry conditions, they show a first linear region and a second concave downward part in which the slope gradually decreases until failure occurs. In saturated conditions, both rocks display a curve with a first small linear region that quickly transforms into a concave downward line with a decreasing slope and a marked non-linearity in the pre-peak region. The critical strain values (strains associated with peak stresses) range from $4.5 \cdot 10^{-4}$ to $6.0 \cdot 10^{-4}$, showing a decrease with water saturation in limestones L-1 and L-3 and an increase in limestone L-2. In addition, in the three limestone lithotypes, the slope of the linear region of the stress-strain curves displays a significant reduction with water saturation.

The mean UTS values obtained in the three limestone lithotypes can be seen in Fig. 6a. Lithotype L-1 exhibited the highest UTS values in both dry and water-saturated conditions (5.64 and 3.27 MPa, respectively).

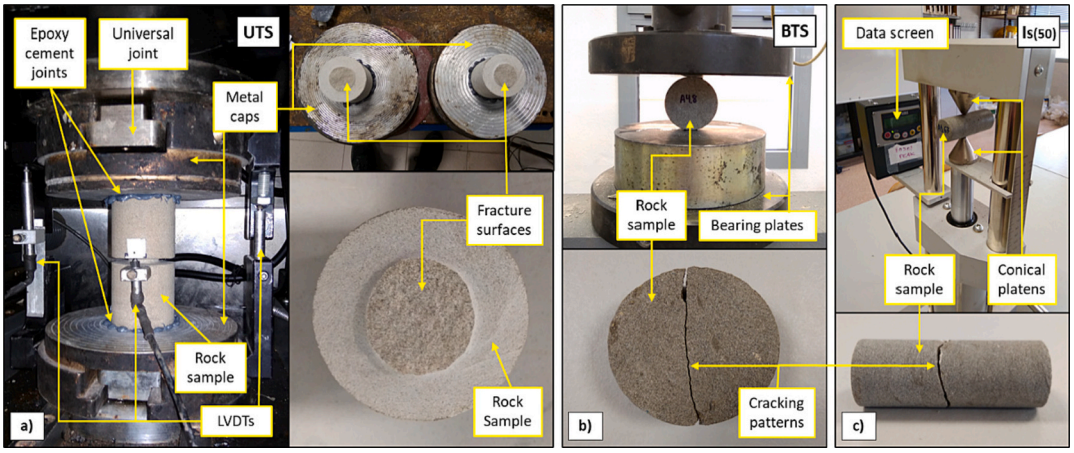

Fig. 4. Test machines, loading setups and typical failure patterns of specimens: (a) uniaxial direct pull test, (b) Brazilian method and (c) point load test.

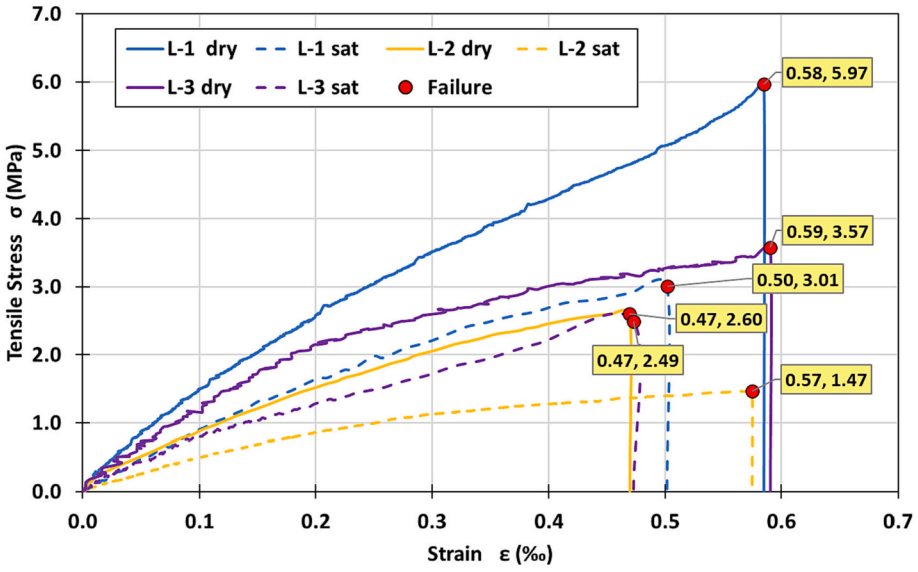

Fig. 5. Representative examples of stress-strain curves obtained in uniaxial tensile direct pull tests for dry and water-saturated specimens of the three limestone lithotypes.

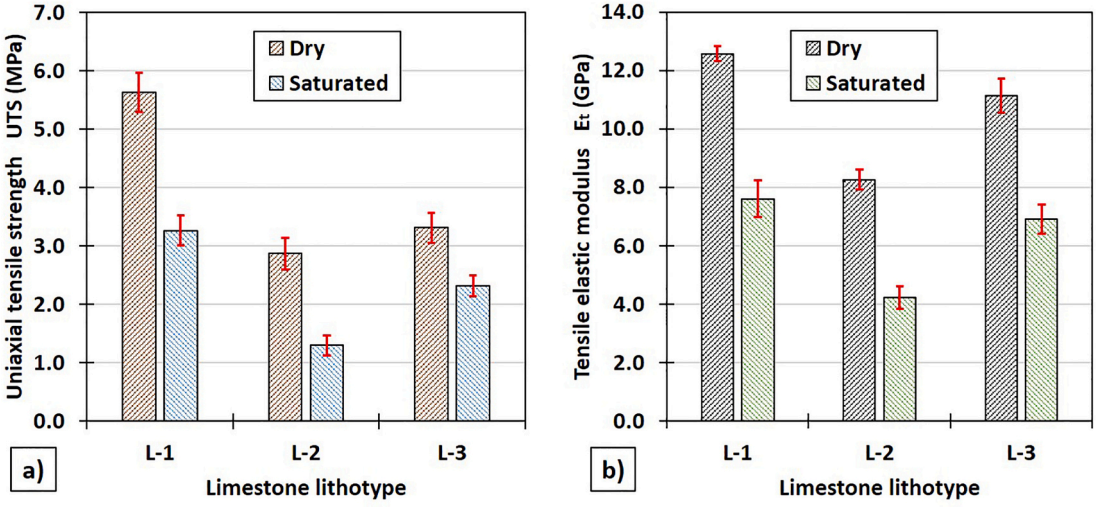

Fig. 6. Comparison of the uniaxial tensile strength (UTS) (a) and the tensile elastic modulus (E_t) (b) values found in dry and water-saturated specimens of the three limestone lithotypes. The error bars represent the standard deviation.

On the contrary, lithotype L-2 showed the lowest UTS values (2.87 and 1.30 MPa, respectively). Lithotype L-3 showed intermediate UTS values, specifically 3.31 MPa in dry state and 2.32 MPa in water-saturated state.

A similar hierarchical order was found in E_t, as can be seen in Fig. 6b. That is, L-1 displayed the largest mean E_t values in both dry and water-saturated conditions (12.58 and 7.61 GPa, respectively) while L-2 presented the smallest mean E_t values (8.26 and 4.23 GPa, respectively). L-3 exhibited intermediate E_t numbers that were close to those found in L-1. In particular, mean E_t values of 11.13 GPa for the dry specimens and 6.92 GPa for the water-saturated ones.

3.2. Brazilian tensile strength (BTS) and point load strength index ($I_{s(50)}$)

Typical examples of the load-displacement curves obtained in Brazilian tests for dry and water-saturated specimens of the three limestone lithotypes are shown in Fig. 7. Three stages can be distinguished in these curves: a) Firstly, a small non-linear stage which corresponds to the closure of microcracks (compaction phase); b) Secondly, a long linear elastic stage in which the bearing load of rock disks increases progressively without apparent signs of instability before they achieve the peak load values; c) Finally, a failure stage in which the rock disks lose their bearing capacity and break abruptly. Furthermore, the displacement corresponding to peak load shows a significant reduction with water saturation in the three lithotypes, which indicates that the presence of water causes a decrease of the deformation ability of these limestones under diametral compressive forces. Also, the slopes of the curves obtained in water-saturated specimens are slightly lower than those found in dry specimens.

The mean BTS values obtained in the three limestone lithotypes are depicted in Fig. 8a. Lithotype L-1 displayed the greatest BTS values in both dry and water-saturated states (6.51 and 3.40 MPa, respectively). By contrast, lithotype L-2 exhibited the smallest BTS values (3.70 and 1.76 MPa, respectively). Lithotype L-3 showed medium BTS values, more precisely 4.89 MPa in dry condition and 2.71 MPa in water-saturated condition.

The mean $I_{s(50)}$ values found in the three limestone lithotypes are represented in Fig. 8b. On the one hand, L-1 showed the highest mean $I_{s(50)}$ values in both dry and water-saturated conditions (3.74 and 2.26 MPa, respectively). On the other hand, L-2 presented the lowest mean $I_{s(50)}$ values (2.04 and 0.90 MPa, respectively). L-3 exhibited intermediate values, particularly, mean $I_{s(50)}$ values of 2.72 MPa for the dry samples and 1.86 MPa for the water-saturated ones.

3.3. Water-induced changes in tensile parameters

Water saturation led to substantial reductions in tensile properties in the three limestone lithotypes. Particularly, limestone L-2 was the most vulnerable to water, exhibiting decreases of 55% in UTS, 49% in E_t, 52% in BTS and 56% in $I_{s(50)}$. By contrast, limestone L-3 was the least sensitive to water, showing decreases of 30% in UTS, 38% in E_t, 45% in BTS and 32% in $I_{s(50)}$. Limestone L-1 exhibited an intermediate water-induced mechanical weakening, displaying drops of 42% in UTS, 40% in E_t, 48% in BTS and 40% in $I_{s(50)}$. A comparison of the softening coefficients (K_{UTS}, K_{Et}, K_{BTS} and $K_{Is(50)}$) found in the three limestone lithotypes can be seen in Fig. 9.

3.4. Relationships correlating UTS with BTS and with $I_{s(50)}$

Significantly different R_{UB} values (UTS/BTS) were obtained for each limestone and each moisture condition. L-1 exhibited higher R_{UB} values than the other two lithotypes in both dry and saturated states (0.87 and 0.96, respectively). In addition, L-3 displayed very dissimilar R_{UB} values between dry and water-saturated specimens (0.68 and 0.85, respectively) while L-2 limestone presented close values for both moisture conditions (0.78 and 0.74, respectively). Furthermore, the regression analysis shown in Fig. 10a allowed to establish the following through-the-origin linear correlation function between both tensile properties for the three lithotypes as a whole:

$$UTS = 0.8155 \cdot BTS \quad (1)$$

where UTS and BTS are both expressed in the same units. The statistical metrics of this linear model were: a mean absolute percentage error (MAPE) of 10.23%, a mean absolute error (MAE) of 0.31, a mean square error (MSE) of 0.14 and a coefficient of determination (R^2) of 0.9875.

Concerning R_{UI} (UTS/$I_{s(50)}$), limestone L-3 presented the smallest values in dry and saturated conditions (1.22 and 1.25, respectively). On the contrary, limestone L-1 displayed the greatest R_{UI} values in both moisture states (1.51 and 1.45, respectively). Limestone L-2 exhibited intermediate R_{UI} numbers, specifically values of 1.40 for the dry samples and 1.45 for the water-saturated ones. Also, the subsequent through-the-origin linear function correlating UTS and $I_{s(50)}$ with a MAPE of 6.91%, a MAE of 0.22, a MSE of 0.08 and a R^2 of 0.9927 was established (Fig. 10b):

$$UTS = 1.3975 \cdot I_{s(50)} \quad (2)$$

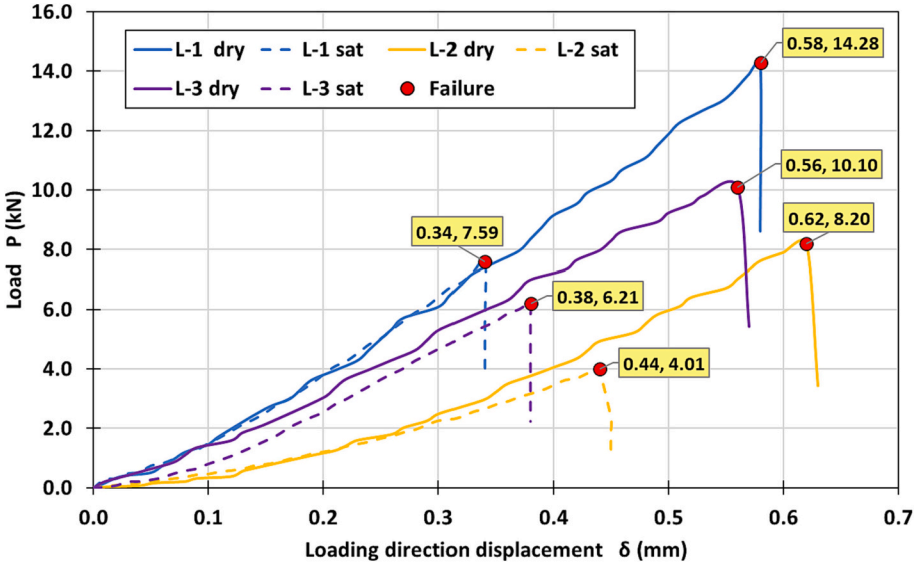

Fig. 7. Representative examples of load-displacement curves obtained in Brazilian tests for dry and water-saturated specimens of the three limestone lithotypes.

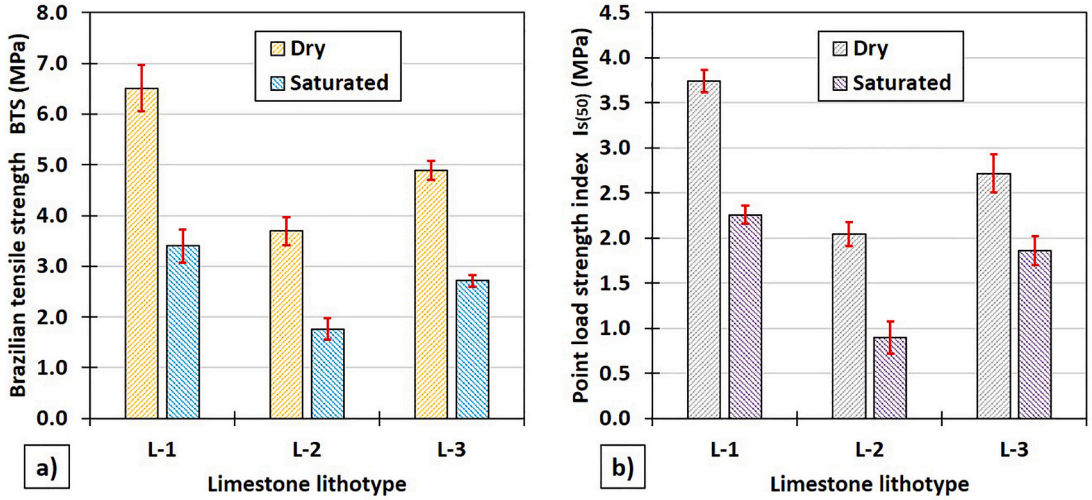

Fig. 8. Comparison of the Brazilian tensile strength (BTS) (a) and the point load strength index ($I_{s(50)}$) (b) values found in dry and water-saturated specimens of the three limestone lithotypes. The error bars represent the standard deviation.

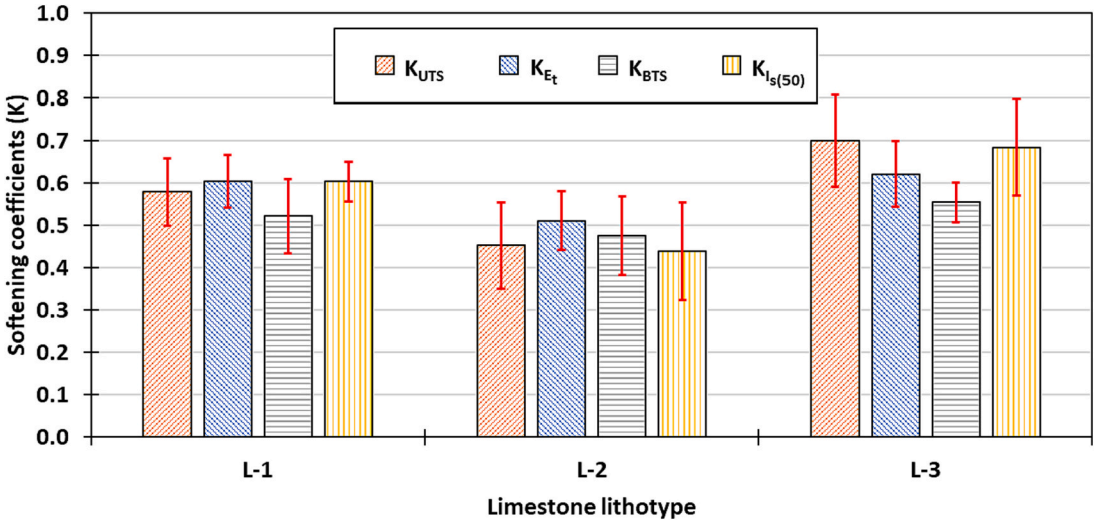

Fig. 9. Softening coefficients obtained in the three tested limestone lithotypes. The error bars represent the standard deviation.

where UTS and $I_{s(50)}$ are both expressed in the same units.

3.5. Relationships correlating E_t with BTS and with $I_{s(50)}$

The values of the ratio between E_t and BTS (R_{EB}) varied considerably depending on limestone lithotype and moisture condition. On the one hand, limestone L-1 showed the lowest R_{EB} values in both dry and water-saturated states (1.93 and 2.24, respectively). On the other hand, limestone L-3 displayed the highest R_{EB} values in both moisture conditions (2.27 and 2.55, respectively). Limestone L-2 exhibited intermediate values, precisely values of 2.23 for the dry specimens and 2.40 for the water-saturated ones. In addition, the regression analysis represented in Fig. 11a provided a general through-the-origin linear relationship between E_t and BTS applicable to the three limestone lithotypes:

$$E_t = 2.1464 \cdot BTS \quad (3)$$

where E_t and BTS are expressed in GPa and MPa, respectively. The statistical metrics of this model were a MAPE of 8.53%, a MAE of 0.70, a MSE of 0.66 and a R^2 of 0.9917.

Regarding the ratio between E_t and $I_{s(50)}$ (R_{EI}), limestone L-1 showed the lowest values, which were almost identical for both dry and water-saturated specimens (3.36 and 3.37, respectively). By contrast, limestone L-2 exhibited significantly different R_{EI} numbers for each moisture condition (4.04 and 4.70, respectively). For its part, L-3 displayed R_{EI} values of 4.09 and 3.72 for the dry and water-saturated samples, respectively. Also, the following through-the-origin linear function with a MAPE of 10.19%, a MAE of 0.80, a MSE of 0.76 and a R^2 of 0.9904 (Fig. 11b) was derived in order to correlate both parameters for the whole set of limestones:

$$E_t = 3.6662 \cdot I_{s(50)} \quad (4)$$

where E_t and $I_{s(50)}$ are expressed in GPa and MPa, respectively.

3.6. Relationship correlating E_t with UTS

The ratio between the two parameters derived from the uniaxial direct pull tests, R_{EU} (E_t/UTS) was calculated for each limestone lithotype and moisture condition. In dry state, the obtained R_{EU} values were 2.23 in L-1, 2.88 in L-2 and 3.36 in L-3. Under a water-saturated state, the measured R_{EU} values were 2.33 in L-1, 3.25 in L-2 and 2.99 in L-3. In

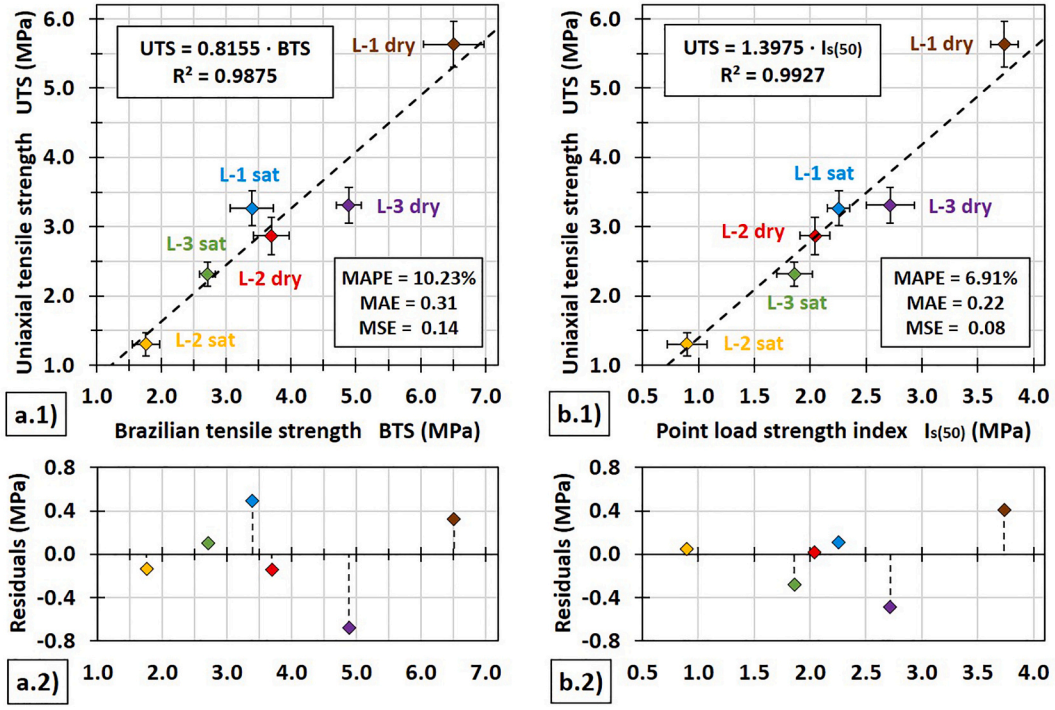

Fig. 10. Relationships correlating uniaxial tensile strength (UTS) with Brazilian tensile strength (BTS) (a.1) and with point load strength index ($I_{s(50)}$) (b.1) found in tested limestones, and their corresponding residual plots (a.2 and b.2, respectively). The error bars represent the standard deviation.

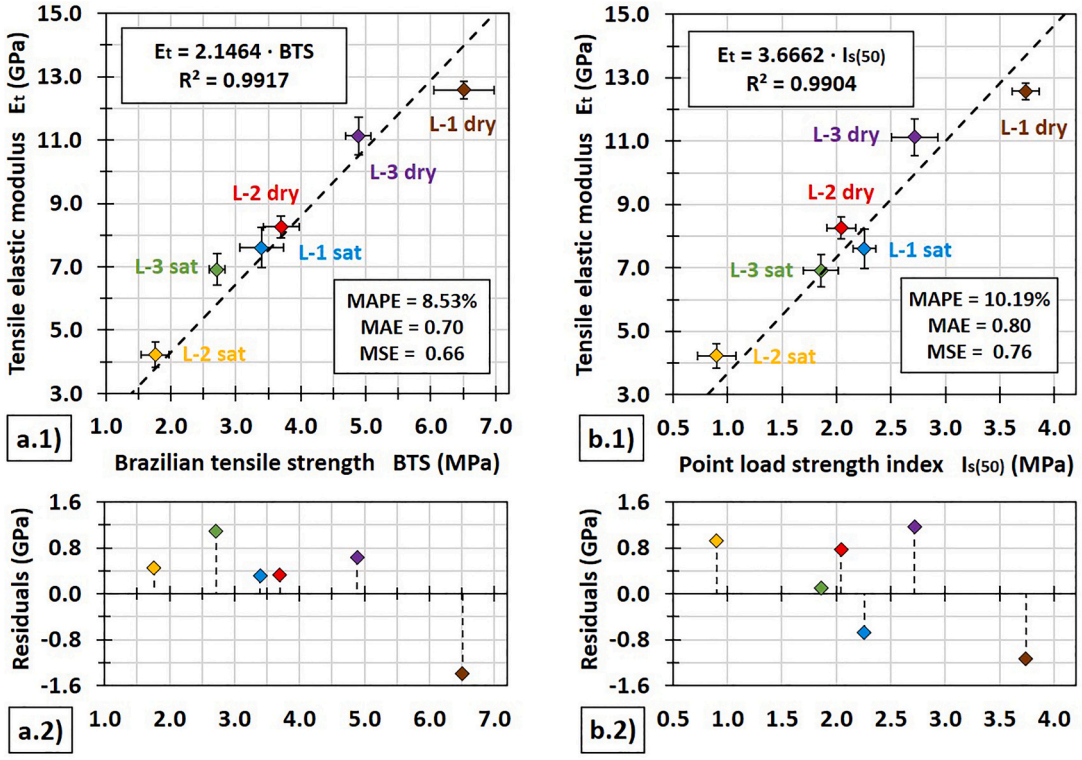

Fig. 11. Relationships correlating tensile elastic modulus (E_t) with Brazilian tensile strength (BTS) (a.1) and with point load strength index ($I_{s(50)}$) (b.1) found in tested limestones, and their corresponding residual plots (a.2 and b.2, respectively). The error bars represent the standard deviation.

addition, a through-the-origin linear function with a MAPE of 15.64%, a MAE of 1.34, a MSE of 2.26 and a R^2 of 0.9713 was proposed to correlate both properties for the entire set of tested limestones (Fig. 12a):

$$E_t = 2.5886 \cdot UTS \quad (5)$$

where E_t and UTS are expressed in GPa and MPa, respectively.

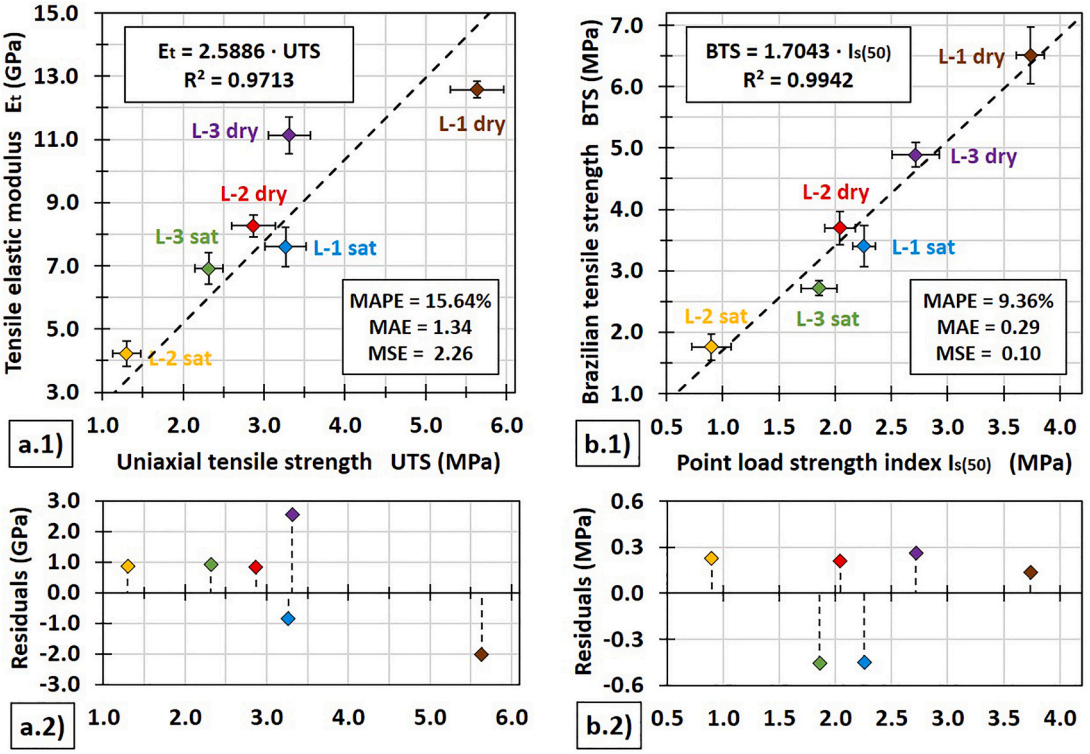

Fig. 12. Relationships correlating tensile elastic modulus (E_t) with uniaxial tensile strength (UTS) (a.1) as well as Brazilian tensile strength (BTS) with point load strength index ($I_{s(50)}$) (b.1) found in tested limestones and their corresponding residual plots (a.2 and b.2, respectively). The error bars represent the standard deviation.

3.7. Relationship correlating BTS with $I_{s\ (50)}$

Although BTS and $I_{s(50)}$ are indexes mainly used to indirectly estimate the tensile and compressive strength properties of rocks, examining the value of the ratio between both parameters (R_{BI}) could also be of interest. In this connection, limestone L-2 displayed the highest R_{BI} values for both dry and water-saturated conditions (1.81 and 1.96, respectively) while the other two lithotypes exhibited quite close R_{BI} numbers to each other. In particular, in dry conditions, L-1 and L-3 showed R_{BI} values of 1.74 and 1.80, respectively. In water-saturated conditions, they presented R_{BI} numbers of 1.51 and 1.46, respectively. Furthermore, the regression analysis depicted in Fig. 12b allowed to obtain the following through-the-origin linear relationship between both parameters that can be globally applied for the three lithotypes:

$$BTS = 1.7043 \cdot I_{s(50)} \quad (6)$$

where BTS and $I_{s(50)}$ are both expressed in the same units. The values of the statistical metrics of this model were: a MAPE of 9.36%, a MAE of 0.29, a MSE of 0.10 and a R^2 of 0.9942.

4. Discussion

In this research, the tensile behaviour of three porous limestones in dry and water-saturated states has been studied using two different approaches: by conducting direct tensile tests and by means of indirect methods (i.e. Brazilian and point load tests). This has enabled us to assess the water-induced variations in different tensile parameters as well as to establish significant relationships between the main tensile properties (UTS and E_t) and the indirect indexes (BTS and $I_{s(50)}$). In this section, the obtained results are compared with those reported in previous works. Also, the findings are discussed by linking the tensile parameters and their water-induced weakening with physical and microstructural properties of tested rocks.

Mechanical characterization revealed that tested limestones are weak rocks that display significant differences in their tensile behaviour. In particular, L-1 exhibits considerably higher values of all measured tensile parameters (UTS, E_t, BTS and $I_{s(50)}$) than the other two lithotypes under both dry and saturated conditions. This result can be attributed to the fact that lithotypes L-2 and L-3 have lower density and larger porosity than lithotype L-1 (La Russa et al., 2015). This finding is also in agreement with preceding studies carried out on these rock types by Rabat et al. (2020c), in which the authors observed that lithotype L-1 displayed greater values of uniaxial and triaxial compressive strength, cohesion and internal friction angle than the others.

Furthermore, a dissimilar water-induced weakening in the measured tensile parameters has been found in each lithotype, which could be related to their different petrological properties. Specifically, the fact that lithotype L-2 presented the greatest reductions in UTS, E_t, BTS and $I_{s\ (50)}$ could be attributed to its larger microfabric and texture variability (wide range of size of its mineral grains) (Pápay and Török, 2018), its high porosity and its low strength and stiffness (Bell, 1978; Romana and Vásárhelyi, 2007). On the contrary, the smallest reductions in the tensile properties obtained in lithotype L-3 could be associated with the presence of a strong cementation between its mineral grains (Anania et al., 2012). Also, the effect of water on the peak deformation (or displacement) was different in direct and indirect tests. In the uniaxial direct pull test, the deformation ability seems to be water-altered in a minor way and without a clear pattern. This result is in accordance with preceding research, in which both increases and decreases of the peak deformation have been reported (Hashiba and Fukui, 2015; Zhu et al., 2022). In Brazilian tests, water caused a sharp reduction in the peak displacements of all tested limestone lithotypes, which is in line with the findings observed in fine-grained sandstones by Zhou et al. (2016).

Fig. 13 shows the relationships between the water-saturated and dry values of each measured tensile property for the entire set of tested limestones in order to derive their corresponding global softening coefficients (K_{UCS}, K_{Et}, K_{BTS} and $K_{Is(50)}$), as well as to compare them with

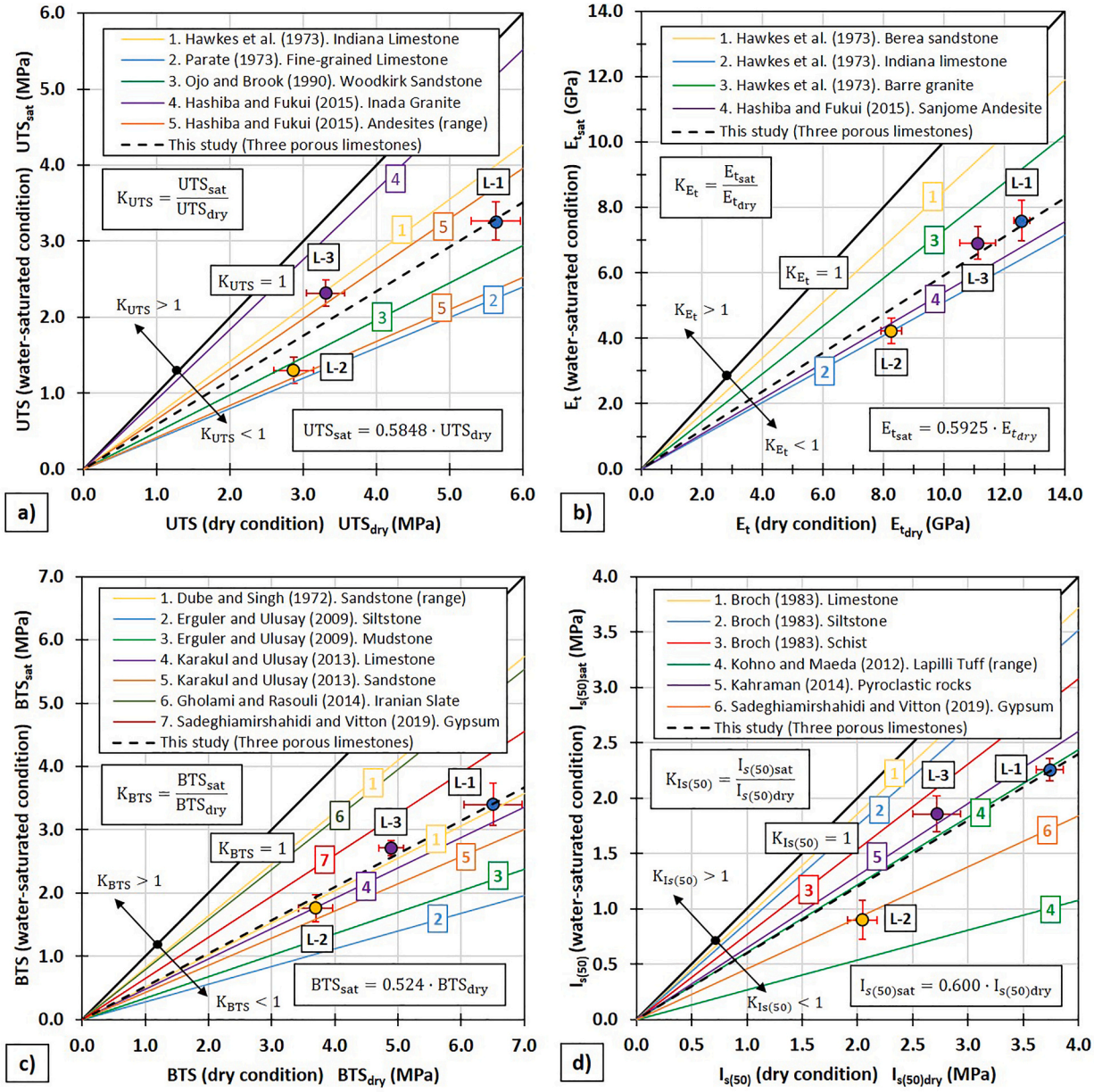

Fig. 13. Global softening coefficients of the tensile properties obtained for the entire set of tested limestones and comparison with the values reported in previous studies: K_{UTS} (a), K_{Et} (b), K_{BTS} (c) and $K_{Is(50)}$ (d). The error bars represent the standard deviation.

those found by previous researchers. Regarding these relationships, it should be noted that global softening coefficients (K) values close to 1 indicate no changes induced by saturation (i.e. the rock is not sensitive to water content changes). In contrast, low values of K indicate a reduction of the considered properties due to the saturation of the rock. Finally, global softening coefficients higher than 1 (i.e. those indicating an increase on mechanical properties caused by the saturation of the rock) have not been reported in the scientific literature.

The through-the-origin linear fit performed for the dry and water-saturated UTS values (Fig. 13a) provides a K_{UTS} number (slope of the line) equal to 0.58, which is lower than the values reported in Inada granite (i.e. K_{UTS} = 0.92) (Hashiba and Fukui, 2015) and Indiana limestone (i.e. K_{UTS} = 0.71) (Hawkes et al., 1973), higher than the numbers obtained in Woodkirk sandstone (i.e. K_{UTS} = 0.49) (Ojo and Brook, 1990) and fine-grained limestone (i.e. K_{UTS} = 0.40) (Parate, 1973), and that falls within the range of values found in andesites (i.e. K_{UTS} = 0.42–0.66) (Hashiba and Fukui, 2015).

Similarly, the line of fit that correlates the water-saturated and dry E_t values (Fig. 13b) returns a global K_{Et} number equal to 0.59, which is smaller than the values measured in Berea sandstone (i.e. K_{Et} = 0.85) and Barre granite (i.e. K_{Et} = 0.73), greater than the number measured in Indiana limestone (i.e. K_{Et} = 0.51) (Hawkes et al., 1973) and quite similar to the value found in Sanjome andesite (i.e. K_{Et} = 0.54) (Hashiba and Fukui, 2015).

Concerning the ratio between water-saturated and dry BTS values, the through-the-origin linear fit (Fig. 13c) gives a global K_{BTS} number equal to 0.52, which is higher than the values reported in Turkish siltstone (i.e. K_{BTS} = 0.28), mudstone (i.e. K_{BTS} = 0.34) (Erguler and Ulusay, 2009), sandstone (i.e. K_{BTS} = 0.43) and limestone (i.e. K_{BTS} = 0.48) (Karakul and Ulusay, 2013), lesser than the numbers obtained in slate (i.e. K_{BTS} = 0.79) (Gholami and Rasouli, 2014) and gypsums (i.e. K_{BTS} = 0.65) (Sadeghiamirshahidi and Vitton, 2019), and that is within the range of values found in sandstone (i.e. K_{BTS} = 0.51–0.82) by Dube and Singh (1972).

With regard to the relationship between water-saturated and dry $I_{s(50)}$ values, the through-the-origin linear fit (Fig. 13d) provides an

overall $K_{Is(50)}$ number equal to 0.60, which is relatively close to the value obtained in pyroclastic rocks (i.e. $K_{Is(50)} = 0.65$) (Kahraman, 2014) and some lapilli tuffs (i.e. $K_{Is(50)} = 0.27–0.61$) (Kohno and Maeda, 2012) and lower than the numbers found in limestone (i.e. $K_{Is(50)} = 0.93$), siltstone (i.e. $K_{Is(50)} = 0.88$) and schist (i.e. $K_{Is(50)} = 0.77$) from Norway (Broch, 1983).

Several mechanisms have been proposed in scientific literature to justify the water-induced weakening of rocks, such as physicochemical changes, pore pressure increase, capillary tension reduction, fracture energy decrease or frictional reduction (Van Eeckhout, 1976). These mechanisms could act in a coupled manner, so establishing a general explanation for the tensile softening observed in tested limestones is challenging. Nevertheless, their mineralogical composition, their petrological characteristics as well as the loading conditions can help to discern which ones are the most relevant. In this sense, failure of a rock specimen under pure tensile stress is principally the consequence of overcoming the cohesion between the mineral grains on potential failure surface and friction produced (Zhu et al., 2022).

Tested rocks are mainly made up of calcite grains and sparitic cement, so their partial dissolution might generate both an increase in porosity and intergranular decohesion and, consequently, their debilitation (Ciantia et al., 2015). Nevertheless, due to the samples were exposed to water during a short time period and calcite dissolution is a very slow process (Risnes et al., 2005; Zhu et al., 2022), these phenomena cannot be the responsible for such a marked tensile softening. In the same vein, the three limestone lithotypes are constituted by modest quantities of quartz and a scarce portion of phyllosilicates (clay minerals), so the stress corrosion phenomenon typically reported in silica-rich rocks (Atkinson and Meredith, 1981; Cai et al., 2019; Michalske and Freiman, 1982) as well as the microstructural damage associated to the swelling of clay minerals (Jiang et al., 2014) might have played only a small role in the obtained mechanical deterioration. Also, it seems clear that the measured UTS and E_t reductions cannot be attributed to an increase in pore pressure because, under uniaxial tensile regime, the pore water can easily migrate towards the newly formed microcracks and the extended pore space generated during loading (Zhu et al., 2022). In fact, this weakening mechanism, which is associated to the incompressibility of the pore water, would be restricted to occur in saturated rocks subjected to confined compressive regimes (Wasantha and Ranjith, 2014).

Hence, the water-induced tensile mechanical weakening observed in tested limestones would be mainly caused by fracture energy decrease, frictional reduction and capillary tension reduction. Fracture energy decrease explanation is founded on Griffith's fracture criterion. This theory argues that when water molecules get in contact with rock surfaces, the specific surface energy diminishes and, as a result, the tensile stress required to generate the crack growth drop (Rehbinder and Shchukin, 1972). Frictional reduction is related to the development of lubricating water films between mineral grains located in primary flaws and pores, which promotes the occurrence of crystal particle slips in direction parallel to the loading direction through potential failure surfaces (Sakuma, 2013; Zhu et al., 2022). Capillary tension reduction has been a widely used hypothesis to explain the water-induced mechanical deterioration found in porous rocks (Taibi et al., 2009). According to this view, when pores are filled by water, the surface tension strongly decreases, which means that the additional friction resistance provided by the contact pressure between grains vanishes (Papamichos et al., 1997).

The values of the ratios between the different tensile mechanical parameters were obtained for the whole set of tested porous limestones by calculating the slopes of the corresponding through-the-origin linear correlation functions. On the one hand, the derived R_{UB} and R_{EB} values can be useful to estimate their pure tensile parameters (UTS and E_t) by using the Brazilian test, which is an easy and quick laboratory method that does not require the use of sophisticated equipment (Efe et al., 2021). Furthermore, according to Lewis (2012), the forecast performances of the proposed fitting models are "highly accurate", since they achieved values of MAPE lower than 11% and of R^2 higher than 0.98.

Complementary regression analyses were carried out by examining the literature information compiled in Table 1 and own data, finding global R_{UB} values of 0.79 for all natural rocks and of 0.81 for the sedimentary ones. The forecast performances of these fitting models are "good" (Lewis, 2012), since they reached MAPE lower than 20% and R^2 higher than 0.95 (Fig. 14).

On the other hand, the derived R_{UI} and R_{EI} values enable to assess indirectly and with "high accuracy" (MAPE lower than 11% and R^2 on the order of 0.99) their pure tensile properties by means of PLT, which is a cheap and rapid test that can be carried out both in the field and in the laboratory and that does not require the use of specimens with strict dimensions and shapes (Kohno and Maeda, 2012). This result comprises a novel contribution to the rock mechanics area, since relationships between these parameters have not been proposed until now.

Additionally, an excellent correlation was found between both indirect tensile indexes (BTS and $I_{s(50)}$) (MAPE lower than 10% and R^2 on the order of 0.99). Specifically, the derived R_{BI} value (1.70) was close to those found in saturated gypsums (2.39) (Sadeghiamirshahidi and Vitton, 2019) as well as in a large variety of Turkish rocks (2.30) (Sulukcu and Ulusay, 2001).

5. Conclusions

Based on the laboratory data and its subsequent analysis, the following conclusions can be derived from this research:

(1) Water saturation caused very significant reductions in direct and indirect tensile strength parameters of porous limestones (30–56%). This water-induced tensile weakening was dissimilar in each lithotype due to their different petrological and physical properties. In addition, loading regime, microstructure and mineralogical composition suggested that this effect can be mainly attributed to the joint action of three mechanisms: fracture energy decrease, frictional reduction and capillary tension decrease.

(2) The regression analyses performed have provided highly accurate through-the-origin relationships between direct tensile strength parameters (UTS and E_t) and the indirect ones (BTS and $I_{(50)}$) for the whole set of tested rocks. Therefore, cheap, rapid and versatile methods such as Brazilian and point load tests can be used to indirectly determine the pure tensile behaviour of these limestones. This result is of paramount importance due to the great difficulties to conduct direct pull tests in rocks.

(3) New general through-the-origin relationships between direct tensile strength parameters (UTS) and the indirect Brazilian tensile strength (BTS) of all type of rocks and sedimentary rocks, based on the joint analysis of available literature data, have been proposed.

In summary, this research broadens knowledge on the direct tensile behaviour of porous limestones and its water-induced variations. In addition, the proposed correlations enable the assessment of these important geomechanical parameters by means of versatile and well-known indirect tests. Future studies could aim at extending the analysis to partially water-saturated samples and other lithologies.

CRediT authorship contribution statement

Álvaro Rabat: Conceptualization, Data curation, Formal analysis, Funding acquisition, Investigation, Methodology, Writing – original draft, Writing – review & editing, Project administration. **Roberto Tomás:** Conceptualization, Supervision, Funding acquisition, Writing – review & editing. **Miguel Cano:** Conceptualization, Supervision,

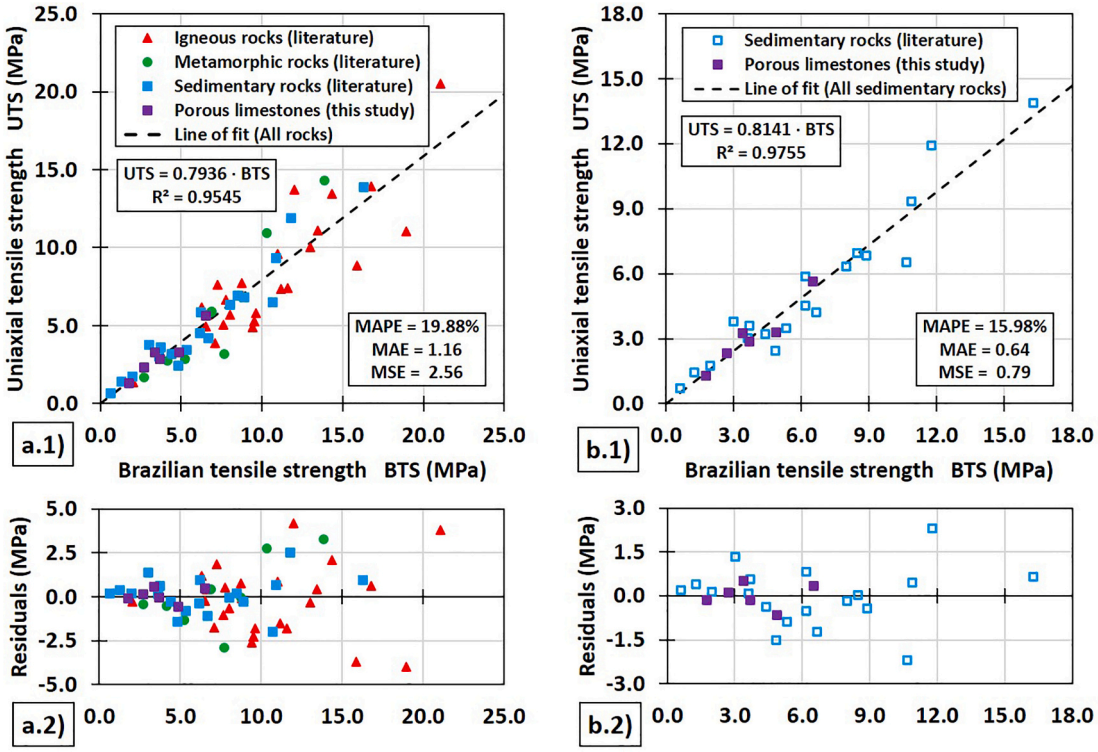

Fig. 14. Relationships correlating uniaxial tensile strength (UTS) with Brazilian tensile strength for all natural rock types (a.1) and for sedimentary rocks (b.1) established from the analysis of literature data (Table 1) and own dataset. Corresponding residual plots (a.2 and b.2, respectively).

Funding acquisition, Writing – review & editing.

Declaration of Competing Interest

The authors declare that they have no known competing financial interests or personal relationships that could have appeared to influence the work reported in this paper.

Data availability

Data will be made available on request.

Acknowledgements

This work was partially supported by the Vicerrectorado de Investigación y Transferencia del Conocimiento of the University of Alicante through the projects UAEEBB2018-09, UAUSTI18-21, UAUSTI20-20 and UAUSTI19-25 and by the Consellería de Innovación, Universidades, Ciencia y Sociedad Digital in the framework of the project CIAICO/2021/335. The authors thank the company "Bateig Piedra Natural S.A." for providing the rock samples. The authors would also like to express their gratitude to the laboratory technician Carlos Palha (University of Minho) for his help during the development of the uniaxial direct pull tests.

References

Al-Derbi, M.S., De Freitas, M.H., 1999. Use of the boussinesq equation for determining the distribution of stress within a diametrical point load test. Rock Mech. Rock. Eng. 32, 257–265. https://doi.org/10.1007/s006030050047.

Alehossein, H., Boland, J.N., 2004. Strength, toughness, damage and fatigue of rock. In: Structural Integrity and Fracture International Conference (SIF'04). Brisbane, Australia, pp. 1–7.

Anania, L., Badalà, A., Barone, G., Belfiore, C.M., Calabrò, C., La Russa, M.F., Mazzoleni, P., Pezzino, A., 2012. The stones in monumental masonry buildings of the "val di Noto" area: New data on the relationships between petrographic characters and physical-mechanical properties. Constr. Build. Mater. 33, 122–132. https://doi.org/10.1016/j.conbuildmat.2011.12.076.

Andreev, G.E., 1991. A review of the Brazilian test for rock tensile strength determination. Part I: calculation formula. Min. Sci. Technol. 13, 445–456. https://doi.org/10.1016/0167-9031(91)91006-4.

ASTM, 2008. D3967–08: Standard Test Method for Splitting Tensile Strength of Intact Rock Core Specimens. West Conshohocken, ASTM Int. https://doi.org/10.1520/D3967-08.2.

ASTM, 2018a. C880/C880M-18: standard test method for flexural strength of dimension stone. ASTM Int. 1–3 https://doi.org/10.1520/C0880_C0880M-18.

ASTM, 2018b. C99/C99M-18: standard test method for modulus of rupture of dimension stone. ASTM Int. 1–4 https://doi.org/10.1520/C0099_C0099M-18.

Atkinson, B.K., Meredith, P.G., 1981. Stress corrosion cracking of quartz: a note on the influence of chemical environment. Tectonophysics 77, 1–11. https://doi.org/10.1016/0040-1951(81)90157-8.

Bell, F.G., 1978. The physical and mechanical properties of the fell sandstones, Northumberland, England. Eng. Geol. 12, 1–29. https://doi.org/10.1016/0013-7952(78)90002-9.

Berenbaum, R., Brodie, I., 1959. Measurement of the tensile strength of brittle materials [1]. Br. J. Appl. Phys. 10, 281–287. https://doi.org/10.1088/0508-3443/10/6/307.

Brace, W.F., 1964. Brittle fracture of rocks. In: Judd, W.R. (Ed.), Proceedings of the International Conference on State of Stress in the Earth's Crust. Elsevier, New York, pp. 111–174.

Brenne, S., Molenda, M., Stöckhert, F., Alber, M., 2013. Hydraulic and sleeve fracturing laboratory experiments on 6 rock types. In: ISRM International Conference for Effective and Sustainable Hydraulic Fracturing. Brisbane, Australia, pp. 435–436. https://doi.org/10.5772/56301.

Briševac, Z., Kujundžić, T., Čajić, S., 2015. Current cognition of rock tensile strength testing by Brazilian test. Min. Geol. Petrol. Eng. Bull. 30, 101–114. https://doi.org/10.17794/rgn.2015.2.2.

Broch, E., 1983. Estimation of strength anisotropy using the point-load test. Int. J. Rock Mech. Min. Sci. 20, 181–187. https://doi.org/10.1016/0148-9062(83)90942-7.

Broch, E., Franklin, J.A., 1972. The point-load strength test. Int. J. Rock Mech. Min. Sci. Geomech. Abstr. 9, 669–676. https://doi.org/10.1016/0148-9062(72)90030-7.

Cacciari, P.P., Futai, M.M., 2018. Assessing the tensile strength of rocks and geological discontinuities via pull-off tests. Int. J. Rock Mech. Min. Sci. 105, 44–52. https://doi.org/10.1016/j.ijrmms.2018.03.011.

Cai, X., Zhou, Z., Liu, K., Du, X., Zang, H., 2019. Water-weakening effects on the mechanical behavior of different rock types: phenomena and mechanisms. Appl. Sci. 9, 14–28. https://doi.org/10.3390/app9204450.

Ciantia, M.O., Castellanza, R., di Prisco, C., 2015. Experimental study on the water-induced weakening of calcarenites. Rock Mech. Rock. Eng. 48, 441–461. https://doi.org/10.1007/s00603-014-0603-z.

Coviello, A., Lagioia, R., Nova, R., 2005. On the measurement of the tensile strength of soft rocks. Rock Mech. Rock. Eng. 38, 251–273. https://doi.org/10.1007/s00603-005-0054-7.

Dai, F., Xia, K., Tang, L., 2010. Rate dependence of the flexural tensile strength of Laurentian granite. Int. J. Rock Mech. Min. Sci. 47, 469–475. https://doi.org/10.1016/j.ijrmms.2009.05.001.
Demirdag, S., Tufekci, K., Sengun, N., Efe, T., Altindag, R., 2019. Determination of the direct tensile strength of granite rock by using a new dumbbell shape and its relationship with brazilian tensile strength. In: IOP Conference Series: Earth and Environmental Science, pp. 1–12. https://doi.org/10.1088/1755-1315/221/1/012094.
Dube, A., Singh, B., 1972. Effect of humidity on tensile strength of sandstone. J. Mines Met. Fuels 20, 8–10.
Efe, T., Demirdag, S., Tufekci, K., Sengun, N., Altindag, R., 2021. Estimating the direct tensile strength of rocks from indirect tests. Arab. J. Geosci. 14, 1–23. https://doi.org/10.1007/s12517-021-07539-9.
Efimov, V.P., 2009. The rock strength in different tension conditions. J. Min. Sci. 45, 569–575. https://doi.org/10.1007/s10913-009-0071-0.
Erguler, Z.A., Ulusay, R., 2009. Water-induced variations in mechanical properties of clay-bearing rocks. Int. J. Rock Mech. Min. Sci. 46, 355–370. https://doi.org/10.1016/j.ijrmms.2008.07.002.
Fahimifar, A., Malekpour, M., 2012. Experimental and numerical analysis of indirect and direct tensile strength using fracture mechanics concepts. Bull. Eng. Geol. Environ. 71, 269–283. https://doi.org/10.1007/s10064-011-0402-7.
Fairhurst, C., 1961. Laboratory measurements of some physical properties of rock. In: 4th U.S. Symposium on Rock Mechanics (USRMS). American Rock Mechanics Association, Pennsylvania, USA.
Fereidooni, D., 2016. Determination of the Geotechnical Characteristics of Hornfelsic Rocks with a Particular Emphasis on the Correlation between Physical and Mechanical Properties. Rock Mech. Rock. Eng. 49, 2595–2608. https://doi.org/10.1007/s00603-016-0930-3.
Fort, R., Bernabéu, A., García del Cura, M.A., López de Azcona, M.C., Ordóñez, S., Mingarro, F., 2010. La Piedra de Novelda: una roca muy utilizada en el patrimonio arquitectónico. Mater. Constr. 52, 19–32. https://doi.org/10.3989/mc.2002.v52.i266.332.
Franklin, J.A., 1985. Suggested method for determining point load strength. Int. J. Rock Mech. Min. Sci. Geomech. Abstr. https://doi.org/10.1016/0148-9062(85)92327-7.
Franklin, J.A., Dusseault, M.B., 1989. Rock Engineering. McGraw-Hill, New York.
Fuenkajorn, K., Klanphumeesri, S., 2010. Determination of direct tensile strength and stiffness of intact rocks. In: Zhao, Labiouse, Dudt, Mathier (Eds.), ISRM International Symposium - EUROCK 2010. Taylor & Francis Group, Lausanne, Switzerland, pp. 79–82. https://doi.org/10.1201/b10550-15.
Garcia-Fernandez, C.C., Álvarez Fernández, M.I., García-Menéndez, J.R., González-Fuentes, A., Álvarez-Díaz, G., Guerrero-Miguel, D.J., González-González, D., 2016. Nuevo ensayo de caracterización de la resistencia a tracción de materiales rocosos. In: 10º Simposio Nacional de Ingeniería Geotécnica; Reconocimiento, Tratamiento y Mejora Del Terreno. Sociedad Española de Mecánica del Suelo, La Coruña, pp. 157–164.
Gholami, R., Rasouli, V., 2014. Mechanical and elastic properties of transversely isotropic slate. Rock Mech. Rock. Eng. 47, 1763–1773. https://doi.org/10.1007/s00603-013-0488-2.
Gong, F., Zhang, L., Wang, S., 2019. Loading rate effect of rock material with the direct tensile and three brazilian disc tests. Adv. Civ. Eng. 2019, 1–8. https://doi.org/10.1155/2019/6260351.
Gorski, B., 1993. Tensile testing apparatus, 5193396.
Gorski, B., Conlon, B., Ljunggren, B., 2007. Forsmark Site Investigation Determination of the Direct and from Borehole KFM01D.
Grasso, P., Xu, S., Mahtab, A., 1992. Problems and promises of index testing of rocks. In: 33rd U.S. Symposium on Rock Mechanics, pp. 879–888.
Guan, J.F., Hu, X.Z., Xie, C.P., Li, Q.B., Wu, Z.M., 2018. Wedge-splitting tests for tensile strength and fracture toughness of concrete. Theor. Appl. Fract. Mech. 93, 263–275. https://doi.org/10.1016/j.tafmec.2017.09.006.
Hashiba, K., Fukui, K., 2015. Effect of water on the deformation and failure of rock in uniaxial tension. Rock Mech. Rock. Eng. 48, 1751–1761. https://doi.org/10.1007/s00603-014-0674-x.
Hawkes, I., Mellor, M., Gariepy, S., 1973. Deformation of rocks under uniaxial tension. Int. J. Rock Mech. Min. Sci. 10, 493–507. https://doi.org/10.1016/0148-9062(73)90001-6.
Hawkins, A.B., McConnell, B.J., 1992. Sensitivity of sandstone strength and deformability to changes in moisture content. Q. J. Eng. Geol. Hydrogeol. 25, 115–130. https://doi.org/10.1144/GSL.QJEG.1992.025.02.05.
Heidari, M., Khanlari, G.R., Kaveh, M.T., Kargarian, S., 2012. Predicting the uniaxial compressive and tensile strengths of gypsum rock by point load testing. Rock Mech. Rock. Eng. 45, 265–273. https://doi.org/10.1007/s00603-011-0196-8.
Hobbs, D.W., 1965. An assessment of a technique for determining the tensile strength of rock. Br. J. Appl. Phys. 16, 259–268. https://doi.org/10.1088/0508-3443/16/2/319.
Hoek, E., 1964. Fracture of anisotropic rock. J. South. Afr. Inst. Min. Metall. 64, 501–518.
Huang, Z., Zhang, Y., Li, Y., Zhang, D., Yang, T., Sui, Z., 2021. Determining tensile strength of rock by the direct tensile, brazilian splitting, and three-point bending methods: a comparative study. Adv. Civ. Eng. 2021, 1–16. https://doi.org/10.1155/2021/5519230.
ISRM, 1978. Suggested Methods for determining Tensile Strength of Rock Materials. Int. J. Rock Mech. Min. Sci. Geomech. Abstr. 15, 99–103. https://doi.org/10.1016/0148-9062(78)90003-7.
ISRM, 2007. The Complete ISRM Suggested Methods for Rock Characterization, Testing and Monitoring: 1974–2006. Comm. Test. Methods, Int. Soc. Rock Mech. ISRM Turkish Natl. Group, Ankara, p. 3.
Jaeger, J.C., 1967. Failure of rocks under tensile conditions. Int. J. Rock Mech. Min. Sci. Geomech. Abstr. 4, 219–227. https://doi.org/10.1016/0148-9062(67)90046-0.
Jiang, Q., Cui, J., Feng, X., Jiang, Y., 2014. Application of computerized tomographic scanning to the study of water-induced weakening of mudstone. Bull. Eng. Geol. Environ. 73, 1293–1301. https://doi.org/10.1007/s10064-014-0597-5.
Kahraman, S., 2014. The determination of uniaxial compressive strength from point load strength for pyroclastic rocks. Eng. Geol. 170, 33–42. https://doi.org/10.1016/j.enggeo.2013.12.009.
Karakul, H., Ulusay, R., 2013. Empirical correlations for predicting strength properties of rocks from P-wave velocity under different degrees of saturation. Rock Mech. Rock. Eng. 46, 981–999. https://doi.org/10.1007/s00603-012-0353-8.
Kim, E., Changani, H., 2016. Effect of water saturation and loading rate on the mechanical properties of Red and Buff Sandstones. Int. J. Rock Mech. Min. Sci. 88, 23–28. https://doi.org/10.1016/j.ijrmms.2016.07.005.
Klanphumeesri, S., 2010. Direct Tension Testing of Rock Specimens. Suranaree University of Technology.
Kohno, M., Maeda, H., 2012. Relationship between point load strength index and uniaxial compressive strength of hydrothermally altered soft rocks. Int. J. Rock Mech. Min. Sci. 50, 147–157. https://doi.org/10.1016/j.ijrmms.2012.01.011.
La Russa, M.F., Belfiore, C.M., Fichera, G.V., Maniscalco, R., Calabrò, C., Ruffolo, S.A., Pezzino, A., 2015. The behaviour to weathering of the Hyblean limestone in the Baroque architecture of the Val di Noto (SE Sicily): an experimental study on the "calcare a lumachella" stone. Constr. Build. Mater. 77, 7–19. https://doi.org/10.1016/j.conbuildmat.2014.11.073.
Lewis, C.D., 2012. Industrial and Business Forecasting Methods: A Practical Guide to Exponential Smoothing and Curve Fitting. Butterworth-Heinemann.
Li, D., Wong, L.N.Y., 2013. The Brazilian disc test for rock mechanics applications: review and new insights. Rock Mech. Rock. Eng. 46, 269–287. https://doi.org/10.1007/s00603-012-0257-7.
Li, L.R., Deng, J.H., Zheng, L., Liu, J.F., 2017. Dominant frequency characteristics of acoustic emissions in white marble during direct tensile tests. Rock Mech. Rock. Eng. 50, 1337–1346. https://doi.org/10.1007/s00603-016-1162-2.
Liao, J.J., Yang, M.T., Hsieh, H.Y., 1997. Direct tensile behavior of a transversely isotropic rock. Int. J. Rock Mech. Min. Sci. 34, 837–849. https://doi.org/10.1016/s1365-1609(96)00065-4.
Luong, M.P., 1990. Tensile and shear strengths of concrete and rock. Eng. Fract. Mech. 35, 127–135. https://doi.org/10.1016/0013-7944(90)90190-R.
Martin, C.D., 1993. The Strength of Massive Lac du Bonnet Granite around Underground Openings. University of Manitoba.
Mellor, M., Hawkes, I., 1971. Measurement of tensile strength by diametral compression of discs and annuli. Eng. Geol. 5, 173–225. https://doi.org/10.1016/0013-7952(71)90001-9.
Michalske, T.A., Freiman, S.W., 1982. A molecular interpretation of stress corrosion in silica. Nature. https://doi.org/10.1038/295511a0.
Minaeian, B., Ahangari, K., 2017. Prediction of the uniaxial compressive strength and Brazilian tensile strength of weak conglomerate. Int. J. Geo-Eng. 8, 1–11. https://doi.org/10.1186/s40703-017-0056-9.
Ojo, O., Brook, N., 1990. The effect of moisture on some mechanical properties of rock. Min. Sci. Technol. 10, 145–156. https://doi.org/10.1016/0167-9031(90)90158-O.
Okubo, S., Fukui, K., 1996. Complete stress-strain curves for various rock types in uniaxial tension. Int. J. Rock Mech. Min. Sci. Geomech. Abstr. 33, 549–556. https://doi.org/10.1016/0148-9062(96)00024-1.
Ordoñez, S., Louis, M., García Cura, M.A., Fort, R., López de Azcona, M.C., Mingarro, F., 1994. Physical properties and petrographic characteristics of some Bateig stone varieties. In: Oliveira, R., Rodrigues, A.G., Coelho, A.G., Cunha, A.P. (Eds.), 7th International IAEG Congress. Lisboa, pp. 3595–3603.
Ordóñez, S., Fort, R., Garcia del Cura, M.A., 1997. Pore size distribution and the durability of a porous limestone. Q. J. Eng. Geol. 30, 221–230. https://doi.org/10.1144/GSL.QJEG.1997.030.P3.04.
Papamichos, E., Brignoli, M., Santarelli, F.J., 1997. Experimental and theoretical study of a partially saturated collapsible rock. Mech. Cohes. Frict. Mater. 2, 251–278. https://doi.org/10.1002/(SICI)1099-1484(199707)2:3<251::AID-CFM33>3.0.CO;2-%23.
Pápay, Z., Török, Á., 2018. Effect of thermal and freeze-thaw stress on the mechanical properties of porous limestone. Period. Polytech. Civ. Eng. 62, 423–428. https://doi.org/10.3311/PPci.11100.
Parate, N.S., 1973. Influence of water on the strength of limestone. Trans. Soc. Min. AIME 254, 127–131.
Perras, M.A., Diederichs, M.S., 2014. A review of the tensile strength of rock: concepts and testing. Geotech. Geol. Eng. 32, 525–546. https://doi.org/10.1007/s10706-014-9732-0.
Rabat, Á., Cano, M., Tomás, R., Tamayo, E., Alejano, L.R., 2020. Evaluation of strength and deformability of soft sedimentary rocks in dry and saturated conditions through needle penetration and point load tests: a comparative study. Rock Mech. Rock. Eng. 53, 2707–2726. https://doi.org/10.1007/s00603-020-02067-6.
Rabat, Á., Cano, M., Tomás, R., 2020a. Effect of water saturation on strength and deformability of building calcarenite stones: correlations with their physical properties. Constr. Build. Mater. 232, 1–15. https://doi.org/10.1016/j.conbuildmat.2019.117259.
Rabat, Á., Tomás, R., Cano, M., 2020b. Evaluation of mechanical weakening of calcarenite building stones due to environmental relative humidity using the vapour equilibrium technique. Eng. Geol. 278, 1–19. https://doi.org/10.1016/j.enggeo.2020.105849.
Rabat, Á., Tomás, R., Cano, M., Miranda, T., 2020c. Impact of water on peak and residual shear strength parameters and triaxial deformability of high-porosity building calcarenite stones: interconnection with their physical and petrological

characteristics. Constr. Build. Mater. 262, 1–20. https://doi.org/10.1016/j.conbuildmat.2020.120789.
Rabat, Á., Tomás, R., Cano, M., 2021. Advances in the understanding of the role of degree of saturation and water distribution in mechanical behaviour of calcarenites using magnetic resonance imaging technique. Constr. Build. Mater. 303, 1–24. https://doi.org/10.1016/j.conbuildmat.2021.124420.
Raj, K., Pedram, R., 2015. Correlations between direct and indirect strength test methods. Int. J. Min. Sci. Technol. 25, 355–360. https://doi.org/10.1016/j.ijmst.2015.03.005.
Ramana, Y.V., Sarma, L.P., 1987. Split-collar tensile test grips for short rock cores. Eng. Geol. 23, 255–261. https://doi.org/10.1016/0013-7952(87)90092-5.
Rao, Q., Liu, Z., Ma, C., Yi, W., Xie, W., 2021. A new flattened cylinder specimen for direct tensile test of rock. Sensors 21, 1–11. https://doi.org/10.3390/s21124157.
Rehbinder, P.A., Shchukin, E.D., 1972. Surface phenomena in solids during deformation and fracture processes. Prog. Surf. Sci. 3, 92–188. https://doi.org/10.1016/0079-6816(72)90011-1.
Risnes, R., Madland, M.V., Hole, M., Kwabiah, N.K., 2005. Water weakening of chalk - Mechanical effects of water-glycol mixtures. J. Pet. Sci. Eng. 48, 21–36. https://doi.org/10.1016/j.petrol.2005.04.004.
Romana, M., Vásárhelyi, B., 2007. A discussion on the decrease of unconfined compressive strength between saturated and dry rock samples. In: Proc. 11th Congr. Int. Soc. Rock Mech, 1, pp. 139–142.
Sadeghiamirshahidi, M., Vitton, S.J., 2019. Mechanical properties of Michigan Basin's gypsum before and after saturation. J. Rock Mech. Geotech. Eng. 11, 739–748. https://doi.org/10.1016/j.jrmge.2018.10.006.
Sakuma, H., 2013. Adhesion energy between mica surfaces: Implications for the frictional coef fi cient under dry and wet conditions, 118, pp. 6066–6075. https://doi.org/10.1002/2013JB010550.
Sari, M., 2018. Investigating relationships between engineering properties of various rock types. Glob. J. Earth Sci. Eng. 5, 1–25. https://doi.org/10.15377/2409-5710.2018.05.1.
Shakoor, A., Barefield, E.H., 2009. Relationship between unconfined compressive strength and degree of saturation for selected sandstones. Environ. Eng. Geosci. 15, 29–40. https://doi.org/10.2113/gseegeosci.15.1.29.
Sulukcu, S., Ulusay, R., 2001. Evaluation of the block punch index test with particular reference to the size effect, failure mechanism and its effectiveness in predicting rock strength. Int. J. Rock Mech. Min. Sci. 38, 1091–1111. https://doi.org/10.1016/S1365-1609(01)00079-X.
Taibi, S., Duperret, A., Fleureau, J.M., 2009. The effect of suction on the hydro-mechanical behaviour of chalk rocks. Eng. Geol. 106, 40–50. https://doi.org/10.1016/j.enggeo.2009.02.012.
Tufekci, K., Demirdag, S., Sengun, N., Altindag, R., Akbay, D., 2016. A new design test apparatus for determining direct tensile strength of rocks. In: ISRM International Symposium - EUROCK 2016. Vigo, Spain, pp. 295–300.
Unlu, T., Yilmaz, O., 2014. Development of a new push-pull direct tensile strength testing apparatus (PPTA). Geotech. Test. J. 37, 1–11. https://doi.org/10.1520/GTJ20130040.
Van Eeckhout, E.M., 1976. The mechanisms of strength reduction due to moisture in coal mine shales. Int. J. Rock Mech. Min. Sci. Geomech. 13, 61–67. https://doi.org/10.1016/0148-9062(76)90705-1.
Vásárhelyi, B., 2005. Statistical analysis of the influence of water content on the strength of the miocene limestone. Rock Mech. Rock. Eng. 38, 69–76. https://doi.org/10.1007/s00603-004-0034-3.
Wang, Y., Deng, J., Li, L., Zhang, Z., 2019. Micro failure analysis of direct and flat loading Brazilian tensile tests. Rock Mech. Rock. Eng. 52, 4175–4187. https://doi.org/10.1007/s00603-019-01877-7.
Wasantha, P.L.P., Ranjith, P.G., 2014. Water-weakening behavior of Hawkesbury sandstone in brittle regime. Eng. Geol. 178, 91–101. https://doi.org/10.1016/j.enggeo.2014.05.015.
Zhang, L., 2017. Chapter 7 - Strength. In: Engineering Properties of Rocks, pp. 251–338. https://doi.org/10.1016/B978-0-12-802833-9.00007-9.
Zhang, Q., Duan, K., Xiang, W., Yuan, S., Jiao, Y., 2018. Direct tensile test on brittle rocks with the newly developed centering apparatus. Geotech. Test. J. 41, 92–102. https://doi.org/10.1520/GTJ20160301.
Zhou, Z., Cai, X., Cao, W., Li, X., Xiong, C., 2016. Influence of water content on mechanical properties of rock in both saturation and drying processes. Rock Mech. Rock. Eng. 49, 3009–3025. https://doi.org/10.1007/s00603-016-0987-z.
Zhu, J., Deng, J., Chen, F., Wang, F., 2022. Failure analysis of water-bearing rock under direct tension using acoustic emission. Eng. Geol. 299, 106541 https://doi.org/10.1016/j.enggeo.2022.106541.